BIOCHEMISTRY
including biophysical chemistry & molecular biology

Article

pubs.acs.org/biochemistry

The Respiratory Syncytial Virus Transcription Antiterminator M_{2-1} Is a Highly Stable, Zinc Binding Tetramer with Strong pH-Dependent Dissociation and a Monomeric Unfolding Intermediate

Sebastián A. Esperante, Lucía B. Chemes, Ignacio E. Sánchez,[†] and Gonzalo de Prat-Gay*

Protein Structure-Function and Engineering Laboratory, Fundación Instituto Leloir and IIBA-Conicet, Patricias Argentinas 435, 1405 Buenos Aires, Argentina

ABSTRACT: The human respiratory syncytial virus M_{2-1} transcription antiterminator is an essential elongation factor required by the RNA polymerase for effective transcription beyond the first two nonstructural genes. Its exclusive presence in pneumovirus among all paramyxovirus suggests a unique function within this small genus. With the aim of understanding its biochemical properties, we investigated this α-helical tetramer by making use of a biophysical approach. We found that the tetramer hydrodynamic radius is considerably extended at high ionic strengths and determined its zinc content to be one atom per monomer. Dissociation−unfolding experiments show a fully reversible and concentration-dependent cooperative transition, but secondary and tertiary structural changes are uncoupled at lower protein concentrations. We detect the presence of a monomeric intermediate, which can be classified as a "late molten globule" with substantial secondary and tertiary structure. Global fittings of experiments from three different probes at two M_{2-1} concentrations provide a free energy of dissociation-unfolding of -36.8 ± 0.1 kcal mol^{-1}, corresponding to a tight dissociation constant of 10^{-28} M^3 at pH 7.0. The tetramer affinity is strongly governed by pH, with a free energy change of 13 kcal mol^{-1} when pH decreases from 7.0 to 5.0 ($K_D = 10^{-18}$ M^3). The drastic changes that take place within a pH range compatible with a cellular environment strongly suggest a regulatory effect of pH on M_{2-1} structure and biochemical properties, likely affecting transcription and interaction with proteins and RNA.

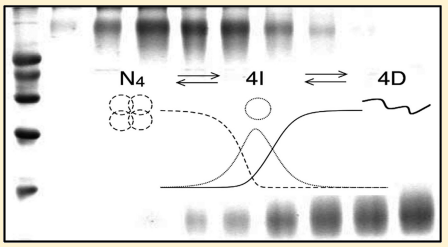

Human respiratory syncytial virus (RSV) is the leading viral cause of pediatric lower-respiratory tract disease and is a significant cause of morbidity and mortality worldwide.[1] This virus belongs to the order Mononegavirales, family Paramyxoviridae, genus *Pneumovirus*.[1] The RSV genome consists of an ~15 kb single-stranded nonsegmented negative-sense RNA, having 10 genes in the following order (3′-NS1-NS2-N-P-M-SH-G-F-M2-L-5′) encoding 11 proteins .The M2 gene is found only in pneumovirus, and the mRNA has two overlapping open reading frames that encode two different proteins, M_{2-1} and M_{2-2}.[1] Coexpression of M_{2-1} along with P, N, and L is essential for the production of infectious RSV from a complete synthetic antigenome.[2] Interestingly, in the closely related human metapneumovirus, coexpression of M_{2-1} is not essential for the recovery of infectious virus in vitro but is essential for virus replication in vivo.[3]

The structural and functional unit for RSV replication and transcription is the polymerase complex, consisting of the genomic RNA and the N, P, and L proteins. In this ribonucleoprotein (RNP) complex, the genomic RNA is tightly bound to the nucleocapsid protein N. RNA replication is directed by the large polymerase protein L and the phosphoprotein P.[4] In infected cells, M_{2-1} is associated with cytoplasmic inclusion bodies that contain N, P, and L proteins[5] through interaction with the RNA[6] and the P protein.[7] In addition, the P−M_{2-1} interaction is important for viral replication.[7]

M_{2-1} is essential for efficient full-length mRNA transcription. M_{2-1} acts as a transcription elongation factor by increasing the processivity of the viral RNA polymerase, preventing premature termination during transcription.[8] Another function of M_{2-1} is to enhance the ability of the polymerase to read through transcription termination signals, thereby acting as a transcription antiterminator.[9] This antiterminator activity varies at the different gene junctions[10] and might be important in determining the amount of polymerase delivered to downstream genes.[9,11]

In addition to its role in transcription, the M_{2-1} protein interacts with the matrix protein M, allowing its incorporation into cytoplasmic inclusion bodies.[5] The M protein inhibits viral transcription and may provide a physical connection between the inclusion bodies and the envelope proteins.[12] Thus, recruitment of the M protein by M_{2-1} might mediate viral assembly and budding.

M_{2-1} is a basic 194-amino acid protein with a theoretical pI of 9.13. It contains a Cys_3His_1 zinc motif at the amino terminus of the protein, between residues 7 and 25. This motif is found in all M_{2-1} proteins of the pneumovirus genus.[1] Other examples of proteins among the mononegaviridae order that harbor this motif are proteins V and C of Sendai virus and the ebola virus

Received: April 29, 2011
Revised: August 25, 2011
Published: August 30, 2011

VP30 transcription activator. It is known that the Cys_3His_1 motif of VP30 binds 1 mol of zinc/mol of protein.[13] This motif is also found in eukaryotic proteins, such as the mammalian nuclear protein Nup475.[14,15] The structure of the Cys_3His_1 motif of the Nup475 protein shows that the zinc ion is coordinated by the conserved cysteines and histidine.[14] Site-directed mutagenesis showed that the Cys_3His_1 motif in M_{2-1} is important for viral growth and for antitermination activity of the protein.[15,16] Alteration of the predicted zinc-coordinating residues resulted in an M_{2-1} protein that was unable to enhance transcriptional readthrough at gene junctions, affected protein phosphorylation, and caused loss of the M_{2-1}−N interaction.[15] However, zinc binding has not been directly demonstrated for M_{2-1} to date.

The interaction of the M_{2-1} and N proteins in cotransfected cells was found to be sensitive to RNase A, indicating that the M_{2-1}−N protein interaction was mediated by RNA.[6] M_{2-1} binds long RNAs with no sequence specificity.[17] The RNA binding domain was mapped between residues 59 and 85, and the Cys_3His_1 motif was not essential for RNA binding activity. M_{2-1} is phosphorylated at residues Ser 58 and Ser 61,[6] and substituting each or both phosphorylation sites decreases the efficiency of M_{2-1} protein transcriptional antitermination activity but does not appear to affect RNA binding.[17]

M_{2-1} functionality has been largely studied using site-directed mutagenesis, transient transfections, and reverse-genetics approaches, but there is only one report that focused on the pure protein in solution.[18] In this work, it was shown that M_{2-1} forms a tetramer of 89 kDa with high α-helical content, and the oligomerization domain was mapped to residues 32−63 using a series of deletion mutants.[18] Mutants lacking this region showed decreased efficiency in RNA transcription, suggesting that oligomerization is essential for the activity of the protein. The M_{2-1} region encompassing residues 59−178 binds to P and RNA in a competitive manner that is independent of the phosphorylation status of the protein.

In this study, we expressed and purified a nonfused version of M_{2-1} in bacteria and investigated its conformational properties and stability in solution. We showed that its predicted zinc binding motif binds 1 mol of zinc/monomer. On the basis of the premise that a dissociation equilibrium of a tight species can be investigated only by perturbation, we used a chemical denaturation approach. We performed unfolding experiments, followed by circular dichroism, fluorescence, glutaraldehyde cross-linking, and size exclusion chromatography, to evaluate the secondary, tertiary, and quaternary structural changes. We quantify different parameters accompanying the transition, propose a model, and discuss it in terms of its possible functional implications.

EXPERIMENTAL PROCEDURES

Expression and Purification of the HRSV Strain A M_{2-1} Protein. The human RSV strain A M_{2-1} sequence was cloned into the BamHI and EcoRI sites of the pRSETA vector as an N-terminally six-His-tagged fusion protein. As a high protein expression level was obtained using this construction in *Escherichia coli* C41(DE3) cells,[19] a modified version of this vector was made to create a bicistronic expression system in which the first open reading frame (ORF) encodes the six-His peptide and the second ORF encodes an unfused version of M_{2-1}. Using inverse polymerase chain reaction mutagenesis,[20] a stop codon (TAG) and a Shine-Dalgarno sequence (AGGAGG) were introduced between the six-His tag and M_{2-1} ORF. The resulting plasmid, HisStop M_{2-1} pRSETA, was sequenced and transformed into *E. coli* strain C41(DE3) for expression.

A single colony was grown in 0.5 L of LB medium at 37 °C containing 100 μg/mL ampicillin. Six hours after inoculation, 0.3 mM IPTG was added to the culture for induction. Cells were harvested by centrifugation 18 h after induction and stored at −70 °C. The pellet was resuspended in 20 mL of buffer [100 mM Tris-HCl (pH 8.0), 0.6 M NaCl, 5 mM 2-mercaptoethanol, and 1 mM EDTA], lysed by sonication, and centrifuged for 30 min at 15000*g* at 4 °C. The resulting supernatant was precipitated via addition of solid ammonium sulfate to 40% saturation. The precipitated protein was collected by centrifugation, resuspended, and dialyzed against buffer A [50 mM Tris-HCl, 0.2 M NaCl, and 1 mM 2-mercaptoethanol (pH 7.0)]. After dialysis, the protein sample was treated with 1 mg of ribonuclease A (Sigma) and incubated for 4 h at 37 °C. The sample was centrifuged at 14000*g* for 20 min at 4 °C, and the soluble fraction was subjected to a Heparin Ceramic HyperD affinity column equilibrated with buffer A. The column was washed with 5 column volumes of the same buffer, and M_{2-1}-bound protein was eluted with a 0.2 to 1.0 M NaCl linear gradient. The M_{2-1} fraction was dialyzed against 50 mM sodium phosphate (pH 7.0), 0.3 M NaCl, and 1 mM DTT.

This procedure yielded ∼50 mg of >95% pure M_{2-1} per liter. The purified protein was stored as a 100 μM solution at −70 °C. Prior to measurement, the protein solutions were subjected to size exclusion chromatography on a Superdex 200 gel filtration column (Pharmacia Biotech) in 50 mM sodium phosphate buffer (pH 7.0), 1 M NaCl, and 1 mM DTT. Protein eluted from this column is >99% pure and was dialyzed against 50 mM sodium phosphate (pH 7.0), 0.3 M NaCl, and 1 mM DTT.

Determination of Protein Concentrations. The M_{2-1} protein stock solution used herein was prepared as follows. Highly purified M_{2-1} was treated for 1 h with 20 mM DTT, dialyzed for 6 h against 50 mM sodium phosphate (pH 7.0), 0.3 M NaCl, 50 μM Zn_2SO_4, and 1 mM DTT, and then dialyzed for 16 h with the same buffer without Zn_2SO_4. The protein concentration was determined spectrophotometrically using a molar extinction coefficient (ε_{280}) of 13200 M^{-1} cm^{-1}, calculated using the Expasy ProtParam tool and in concordance with a previous report.[18] A 260 nm:280 nm ratio of 0.6 was indicative of minimal nucleic acid contamination. The protein concentration is expressed as a monomer concentration.

Size Exclusion Chromatography. Size exclusion chromatography was conducted on a Superdex 200 HR-10/30 (24 mL) column (Pharmacia Biotech). Unfolding gel filtration experiments were conducted on the column equilibrated with the indicated guanidinium chloride (Gdm.Cl) concentration. The samples were incubated for 16 h before injection, and the elution of the protein was monitored at 220 nm. The column was calibrated in 50 mM sodium phosphate (pH 7.0) and 1 M NaCl, with the following standard globular proteins: ferritin (440 kDa), catalase (232 kDa), BSA (67 kDa), ovalbumin (43 kDa), and chymotrypsinogen A (25 kDa) (from a gel calibration kit, Pharmacia Biotech, Uppsala, Sweden). The void volume (V_o) and total volume ($V_o + V_i$) were determined by loading Blue Dextran and acetone, respectively, at each Gdm.Cl concentration to check for column compression.

Light Scattering. The determination of the average molecular mass of M_{2-1} by static light scattering (SLS) was

conducted on a Precision Detectors PD2010 light scattering instrument connected in tandem to a high-performance liquid chromatography system and an LKB 2142 differential refractometer. The 90° light scattering and refractive index signals of the eluting material were recorded on a personal computer and analyzed with Discovery32 that was supplied by Precision Detectors. The determination of the hydrodynamic size distribution of M_{2-1} by dynamic light scattering (DLS) was performed on a Zetasizer Nano S DLS device from Malvern Instruments. The solutions were centrifuged at 14000*g* for 10 min at 4 °C and filtered with Ultrafree-MC microcentrifuge filters (0.22 μm, Millipore) before measurements were taken.

Circular Dichroism (CD) Spectroscopy. Far-UV CD measurements were taken on a Jasco J-810 spectropolarimeter using a Peltier temperature-controlled sample. Spectra between 200 and 260 nm were recorded at a rate of 200 nm/min with a response time of 2 s and a bandwidth of 2 nm. All spectra were an average of at least five scans. Spectra of M_{2-1} at 10 and 1 μM were recorded on 0.1 and 0.5 cm path length cells, respectively. The ellipticity at 260 nm was subtracted from the other ellipticities as a baseline value. The results are expressed as degrees square centimeter per decimole.

Fluorescence Spectroscopy. Fluorescence emission spectra were recorded on a Jasco FP-6500 spectrofluorometer with an excitation wavelength of 295 nm, and the emission spectrum was recorded from 310 to 450 nm. Fluorescence emission data were analyzed by first subtracting the buffer background at the appropriate Gdm.Cl concentration, and the center of spectral mass of the emission spectrum (CM, in cm^{-1}) was quantified as follows:

$$\mathrm{CM} = \sum (\upsilon_i F_i) / \sum F_i \tag{1}$$

where F_i is the fluorescence emission at wavenumber υ_i and the summation is conducted over the range of measured values of *F*. Spectra of M_{2-1} at concentrations of >1 μM were recorded in a 4 mm path length quartz cell and at <1 μM on a 10 mm light path. The excitation and emission slits were set at 5 and 10 nm, respectively. Fluorescence emission spectra for ANS binding were recorded with excitation at 370 nm, with a 5 nm bandpass. The ANS concentration was 100 μM. All data shown are an average of at least five spectra.

Chemical Denaturation and Dissociation Experiments. The stock solutions contained 7.5 M Gdm.Cl or 10 M urea. For unfolding experiments, each sample was incubated for a minimum of 16 h prior to measurement. The Gdm.Cl experiments were conducted again after a 48 h incubation to confirm that the denaturation process had reached equilibrium. For refolding experiments, a concentrated stock solution of M_{2-1} was unfolded in 6 M Gdm.Cl and incubated overnight. The following day, the samples were diluted into gradually decreasing concentrations of the denaturant. All samples were incubated for 16 h prior to measurement. Dissociation experiments were performed by making serial dilutions of M_{2-1} to final concentrations of 0.05−10 μM. All samples were incubated for 16 h prior to measurement.

Glutaraldehyde Cross-Linking. The M_{2-1} protein solutions were incubated for 16 h at a given Gdm.Cl concentration. The samples were then treated with 0.1% glutaraldehyde and incubated for 30 s at room temperature. The reactions were stopped by addition of 100 mM Tris-HCl (pH 7.0) and 50 mM $NaBH_4$. The samples were diluted 10 times with 50 mM sodium phosphate (pH 7.0) and 0.3 M NaCl and precipitated on ice with 10% TCA (trichloroacetic acid) for 30 min. The samples were centrifuged at 14000*g* for 10 min at 4 °C, and the pellet was washed twice with ice-cold acetone and resuspended in 20 μL of sodium dodecyl sulfate (SDS) sample buffer. Finally, the samples were boiled and loaded onto a 12.5% sodium dodecyl sulfate−polyacrylamide gel and stained with Coomasie blue. At least four or five independent glutaraldehyde cross-linking experiments for each M_{2-1} concentration were performed. The pictures of the stained gel were scanned, and ImageJ (http://rsbweb.nih.gov/ij/download.html) was used for densitometric analysis. The results were expressed as the fraction of tetramer.

Modeling of M_{2-1} Equilibrium Unfolding. We considered the following three-state unfolding model with a monomeric intermediate to estimate the thermodynamic parameters for each transition:

$$\mathrm{N_4} \overset{K_{D1}}{\longleftrightarrow} 4\mathrm{I} \overset{K_{D2}}{\longleftrightarrow} 4\mathrm{D} \tag{2}$$

where N_4 is the native tetramer, I is the monomeric intermediate, and D is the denatured monomer. K_{D1} and K_{D2} are the equilibrium constants for the two equilibria and are defined by

$$K_{D1} = \frac{[\mathrm{I}]^4}{[\mathrm{N_4}]};\ K_{D2} = \frac{[\mathrm{D}]}{[\mathrm{I}]} \tag{3}$$

According to this model, the fractional population of each species (f_N, f_I, and f_D) is defined by

$$f_N = \frac{4[\mathrm{N_4}]}{P_t};\ f_I = \frac{[\mathrm{I}]}{P_t};\ f_D = \frac{[\mathrm{D}]}{P_t} \tag{4}$$

where P_t is the total protein concentration. By considering that the sum of the fractional populations f_N, f_I, and f_D equals 1, we obtain the following fourth-order equation:

$$\frac{4P_t^3}{K_{D1}} f_I^4 + (K_{D2} + 1) f_I - 1 = 0 \tag{5}$$

Analytical solution of this equation allows for calculation of the fractional population of the monomeric intermediate (f_I). This solution leads to one relevant real root that is

$$f_I = -\frac{1}{2}\sqrt{-m+n} + \frac{1}{2}\sqrt{m-n+q} \tag{6}$$

with

$$m = [4(2/3)^{1/3}] \Big/ \left[\left(9ab^2 + \sqrt{3} \times \sqrt{27a^2b^4 + 256a^3}\right)^{1/3}\right]$$

$$n = \left[\left(9ab^2 + \sqrt{3} \times \sqrt{27a^2b^4 + 256a^3}\right)^{1/3}\right] / (2^{1/3} \times 3^{2/3} a)$$

$$q = \frac{2b}{a\sqrt{-m+n}}$$

$$a = \frac{4P_t^3}{K_{D1}};\ b = K_{D2} + 1 \tag{7}$$

dx.doi.org/10.1021/bi200661k | *Biochemistry* 2011, 50, 8529–8539

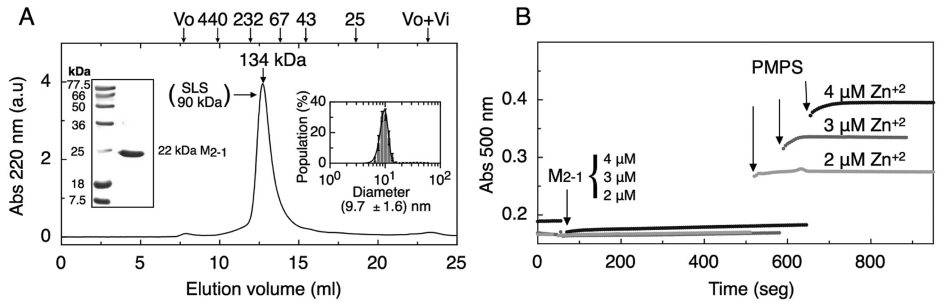

Figure 1. Hydrodynamic and zinc binding properties of M_{2-1}. (A) Size exclusion chromatography of purified M_{2-1} in a Superdex 200 column. The arrows above the graph denote the positions of the void volume (V_o), molecular mass standards in kilodaltons, and total volume ($V_o + V_i$). According to the column calibration, the peak corresponds to a 134 kDa species (indicated above the peak). The average molecular mass of the peak, determined by static light scattering, is indicated (SLS 90 kDa). The left inset shows purified recombinant M_{2-1} in a 12.5% SDS–PAGE gel stained with Coomassie Blue: lane 1, molecular mass markers (kilodaltons); lane 2, purified M_{2-1}. The right inset shows the particle size distribution of 20 μM M_{2-1} in 50 mM sodium phosphate (pH 7.0), 0.3 M NaCl, and 1 mM DTT, measured by DLS. (B) Colorimetric measurement of M_{2-1} protein Zn^{2+} content. Purified M_{2-1} without DTT was added at different concentrations (2, 3, and 4 μM) to a solution containing 100 μM PAR and monitored at 500 nm to measure the formation of the Zn^{2+}–PAR complex. Upon addition of 100 μM PMPS, the release of strongly bound Zn^{2+} was measured, and the content of Zn^{2+} bound to M_{2-1} protein was quantified vs a standard curve. The reactions were performed in 50 mM sodium phosphate (pH 7.0) and 0.3 M NaCl at 20 °C.

The fractions of native tetramer (f_N) and denatured monomer (f_D) can be expressed as a function of f_I:

$$f_D = K_{D2} f_I;\ f_N = \frac{4P_t^3}{K_{D1}} f_I^4 \tag{8}$$

Fluorescence and CD signals were considered to follow the following linear function:

$$y = f_N y_N + f_I y_I + f_D y_D \tag{9}$$

where y_N, y_I, and y_D represent the spectroscopic signals of the native, intermediate, and denatured states, respectively, and f_N, f_I, and f_D their fractional populations. When necessary, observed slopes in the baseline signal were taken into account by considering a linear dependence of the signal on Gdm.Cl concentration. The normalized tetramer fraction obtained from cross-linking experiments was fit as $y = f_N$. The free energy of unfolding was considered to depend linearly on Gdm.Cl concentration and was related to the equilibrium constants K_{D1} and K_{D2} by

$$K_{D1} = e^{-(\Delta G_1^{H_2O} - m_1[\text{Gdm.Cl}])/RT}$$
$$K_{D2} = e^{-(\Delta G_2^{H_2O} - m_2[\text{Gdm.Cl}])/RT} \tag{10}$$

We performed nonlinear global fitting of the far-UV CD, tryptophan center of spectral mass and tetramer fraction signals obtained from equilibrium unfolding experiments performed at 1 and 10 μM M_{2-1} to obtain estimates for the relevant thermodynamic parameters K_{D1}, m_1, K_{D2}, and m_2.

Modeling of M_{2-1} Dissociation. Dissociation experiments were analyzed by considering a simple tetramer–monomer equilibrium:

$$N_4 \overset{K_D}{\leftrightarrow} 4M \tag{11}$$

where the equilibrium constant K_D and the fractional populations of native tetramer (f_N) and monomer (f_M) are

$$K_D = \frac{[M]^4}{[N_4]};\ f_N = \frac{4[N_4]}{P_t};\ f_M = \frac{[M]}{P_t} \tag{12}$$

where P_t is the total protein concentration. By considering that the sum of the fractional populations f_N and f_M equals 1, we can calculate the fraction of monomer (f_M) by solving the following quartic equation, as previously shown by Mateu and Fersht.[21]

$$\frac{4P_t^3}{K_D} f_M^4 + f_M - 1 = 0 \tag{13}$$

The relevant real root of this equation gives the solution for f_M and follows eqs 6 and 7 with a b of 1. The fraction of native tetramer (f_N) is

$$f_N = 1 - f_M \tag{14}$$

The tryptophan fluorescence center of spectral mass signal was fit to the linear function

$$y = f_N y_N + f_M y_M \tag{15}$$

where y_N and y_M represent the spectroscopic signal of the tetrameric and monomeric species, respectively. In dissociation experiments performed at different Gdm.Cl concentrations, data were fit globally by considering a linear dependence of the free energy of dissociation ΔG on Gdm.Cl concentration. ΔG was related to the equilibrium constant K_D by eq 10.

RESULTS

Behavior of the M_{2-1} Protein in Solution. Recombinant human RSV antiterminator M_{2-1} was purified without any tag or fusion protein to high levels of purity (Figure 1A, left inset). Size exclusion chromatography was performed in 50 mM sodium phosphate buffer (pH 7.0) and 1 M NaCl at 20 °C, and the estimated molecular mass derived from the elution volume corresponded to a spherical protein of 134 kDa. However, the weight-average molecular mass monitored by static light scattering was 90 kDa, in agreement with the expected molecular mass for a tetramer (88 kDa) (Figure 1A). Moreover, a dynamic light scattering experiment using 20 μM M_{2-1} showed a highly monodisperse species with a diameter of 9.7 ± 1.6 nm (Figure 1A, right inset), corresponding to a 174 kDa spherical protein.[22] Altogether, these data confirm that M_{2-1} is indeed a tetramer, but with a nonspherical, extended conformation.

dx.doi.org/10.1021/bi200661k | Biochemistry 2011, 50, 8529–8539

Although RSV and MNV M_{2-1} contain a conserved zinc binding motif, the metal content has not been actually measured to date. The amount of bound zinc was determined by spectrophotometric measurement of the metallochromic indicator 4-(2-pyridylazo)resorcinol (PAR)[23] in a time course manner. Purified 2−4 μM M_{2-1} without DTT was first added to a solution containing 100 μM PAR reagent to measure weakly bound metal. No change in absorbance at 500 nm was observed, indicating that there was no weakly bound zinc (Figure 1B). Next, the presence of tightly bound zinc was tested by the addition of 100 μM *p*-hydroxymercuriphenylsulfonate (PMPS). The release of zinc was followed kinetically, and the amount of zinc was quantified against a curve with a standard solution (Figure 1B). An average of five independent measurements indicated that the addition of PMPS released one tightly bound metal atom per monomer. Although more experimental work is required for an accurate measurement of the dissociation constant of this zinc atom, we can conclude that the affinity is higher than that of the $Zn(PAR)_2$ complex ($K_a = 2 \times 10^{12}$ M^{-1}).

Conditions that may modulate the conformational equilibria and stability of M_{2-1} in the cells include pH. We analyzed the effect of pH on M_{2-1} conformation at 20 μM in a broad range buffer with 100 mM Tris-HCl, 50 mM MES, 50 mM sodium acetate, 0.2 M NaCl, and 1 mM DTT at 20 °C. We performed measurements within the pH 3.0−9.0 range and found a sharp transition at pH <5.0 (Figure 2). The unique tryptophan residue of M_{2-1}, located at position 30, provided an ideal probe for investigating conformational transitions. W30 became more exposed to the solvent at the lowest pH values, suggesting at least partial denaturation (Figure 2A and its inset). M_{2-1} secondary structure also showed a transition below pH 5.0, as judged by the change in ellipticity (Figure 2B). However, the typical α-helical far-UV CD spectra of M_{2-1} changed only slightly at pH 3.0, indicating that the protein remained rather folded (Figure 2B, inset). Below the pH 5.0 transition threshold or after incubation for 24 h at pH 5.0, M_{2-1} aggregates to a higher-order soluble oligomeric species (Figure 2C). This higher-order species at pH 3.0 was a large, monodisperse oligomer with a 30 nm diameter (Figure 2C, inset). The oligomer was extremely thermostable and returned to the tetrameric state at pH 7.0 after dialysis (data not shown).

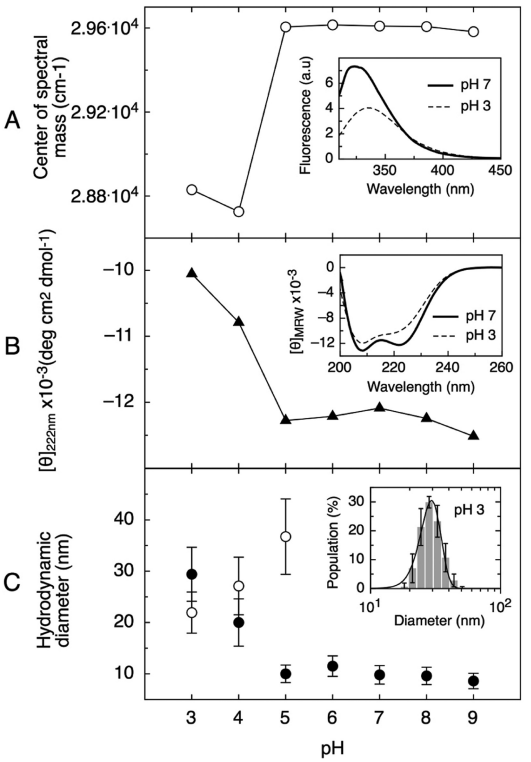

Figure 2. pH-induced conformational changes in the M_{2-1} tetramer. (A) Tryptophan fluorescence spectrum center of spectral mass of M_{2-1} at different pH values. The inset shows tryptophan fluorescence emission spectra of M_{2-1} at pH 7.0 (—) and pH 3.0 (---). (B) Molar ellipticity of M_{2-1} at 222 nm as a function of pH. The inset shows far-UV CD spectra of M_{2-1} at pH 7.0 (—) and pH 3.0 (---). (C) Hydrodynamic diameter of M_{2-1} at different pHs, measured by DLS (●) after incubation for 4 h. Measurements at pH 3.0, 4.0, and 5.0, after incubation for 24 h, are also shown (○). The inset shows the particle size distribution of M_{2-1} at pH 3, measured by DLS. The M_{2-1} protein concentration used for pH dependence experiments was 20 μM in broad range buffer [100 mM Tris-HCl, 50 mM MES, 50 mM sodium acetate, 1 mM DTT, and 0.2 M NaCl (pH 4, 5, 6, 7, 8, and 9)]. The buffer used at pH 3.0 consisted of 50 mM glycine-HCl, 0.3 M NaCl, and 1 mM DTT. All samples were incubated for 4 h prior to measurement and measured at 20 °C.

Urea-Induced M_{2-1} Conformational Transitions. The conformational stability of the M_{2-1} tetramer at equilibrium was investigated by chemical unfolding experiments using the denaturants urea and Gdm.Cl. First, 10 μM M_{2-1} was equilibrated in 50 mM sodium phosphate buffer (pH 7.0) and 1 mM DTT at 20 °C at different urea concentrations, and its conformational properties were studied using tryptophan fluorescence, circular dichroism, and ANS binding (Figure 3A). Urea shifted the center of spectral mass (CM) of fluorescence emission to the red starting at 5.5 M urea, indicative of solvent exposure of the tryptophan residue. This increase was larger than that observed at low pH values. Urea also induced a loss of secondary structure, as shown by the changes in the CD ellipticity signal, but starting at 3.8 M urea. ANS fluorescence showed that this hydrophobic, negatively charged probe bound to the folded state, possibly at the RNA binding site. The ANS fluorescence decreased sharply starting at 1 M urea, suggesting that the RNA binding site is perturbed by urea and/or the dye is displaced by the denaturant.

Changes in the three spectroscopic signals were completely uncoupled from each other (Figure 3A). This clearly indicates that at least one partially folded, intermediate conformation is populated in urea-induced M_{2-1} unfolding. Population of the intermediate peaks at 5 M urea, where the protein showed a significant amount of α-helix (Figure 3B), displayed shielding of W30 from the solvent (Figure 3A) and residual ANS binding (Figure 3A). With the change from 5 to 8 M urea, the protein loses the remaining secondary structure and ANS binding ability and W30 becomes partially exposed to the solvent (Figure 3A,B). Unfortunately, the highest attainable urea concentration did not allow for the determination of an unfolding state baseline, which precluded quantitative analysis of the unfolding transition.

Gdm.Cl-Induced M_{2-1} Unfolding and Dissociation. The conformational equilibria of M_{2-1} were next investigated under the same conditions using Gdm.Cl, a denaturant stronger than urea that combines preferential solvation of hydrophobic side chains with strong electrostatic screening. As expected, Gdm.Cl unfolded the protein at much lower concentrations than urea at the same protein concentration (Figure 3C). A gradual increase in the level of Gdm.Cl shifted the fluorescence spectra to that of a fully exposed conformation at ~2.5 M

dx.doi.org/10.1021/bi200661k | *Biochemistry* 2011, 50, 8529−8539

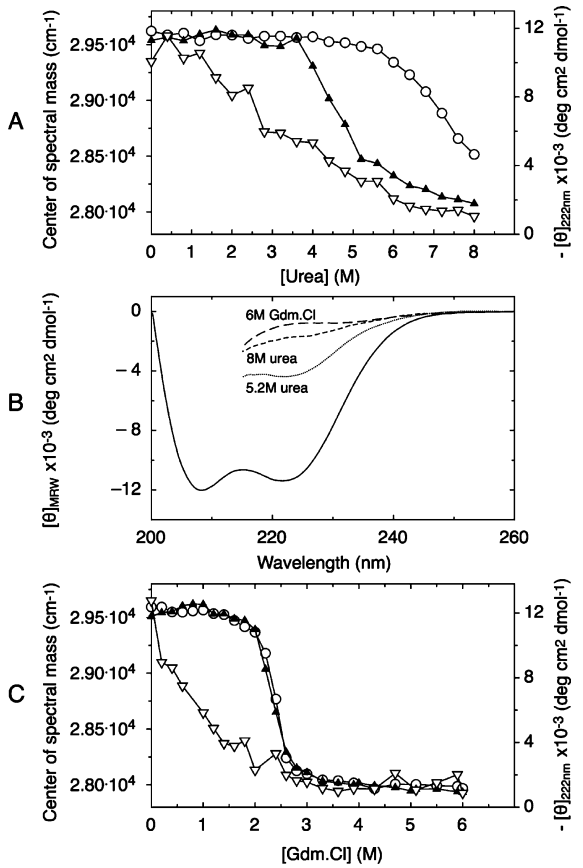

Figure 3. Conformational stability of M_{2-1} in urea and Gdm.Cl. (A) Urea-induced denaturation of M_{2-1} monitored by changes in the center of spectral mass (○), molar ellipticity at 222 nm (▲), and ANS fluorescence intensity at 470 nm (▽). (B) Far-UV CD spectra of native M_{2-1} (—) in 50 mM sodium phosphate (pH 7.0), 0.3 M NaCl, and 1 mM DTT, in 5.2 M urea, in 8 M urea, and the unfolded protein in 6 M Gdm.Cl. (C) Gdm.Cl-induced denaturation of M_{2-1} monitored by changes in the center of spectral mass (○), molar ellipticity at 222 nm (▲), and ANS fluorescence intensity at 470 nm (▽). The M_{2-1} protein concentration for each denaturant point was 10 μM, in 50 mM sodium phosphate (pH 7.0) and 1 mM DTT. All measurements were taken at 20 °C.

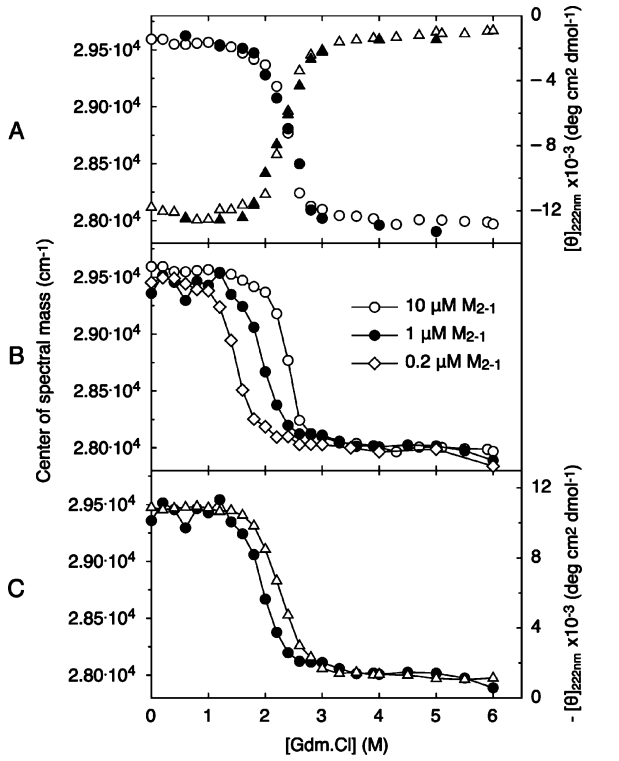

Figure 4. Reversibility and concentration dependence of M_{2-1} Gdm.Cl-induced denaturation. (A) Reversibility of M_{2-1} Gdm.Cl-induced denaturation: M_{2-1} equilibrium denaturation (empty symbols) and renaturation (filled symbols), followed by tryptophan fluorescence center of spectral mass (circles) and far-UV CD (triangles). The protein concentration was 10 μM, and measurements were performed at 20 °C. (B) Concentration dependence of M_{2-1} Gdm.Cl denaturation. Gdm.Cl-induced denaturation was followed by the center of spectral mass at 10 (○), 1 (●), and 0.2 μM (◇) at 20 °C. (C) Uncoupling between secondary and tertiary structural changes. Gdm.Cl-induced denaturation at 1 μM M_{2-1} was followed by changes in molar ellipticity at 222 nm (△) and center of spectral mass (●).

denaturant, concomitant with a decrease in intensity. The absence of an isodichroic point (not shown) suggested the presence of intermediates, which was expected from the urea-induced unfolding results. Gdm.Cl also released ANS from the protein, but starting at 1 M denaturant. In addition, Gdm.Cl caused a complete disappearance of the ellipticity signal at ~2.5 M denaturant, closely following the changes in W30 fluorescence.

Clear baselines could be determined for each signal after the transition, confirming that the Gdm.Cl denaturant was able to completely unfold M_{2-1}, which allowed a quantitative analysis of the unfolding equilibria. Another important requirement for thermodynamic analysis of the data is reversibility of the system. Refolding experiments were conducted such that the protein at high denaturant concentrations was diluted at the indicated Gdm.Cl concentrations. Both ellipticity and fluorescence CM showed complete reversibility (Figure 4A).

Denaturant-induced unfolding of oligomeric proteins is expected to be coupled with dissociation into monomers. The presence of such a dissociation process can be inferred from the protein concentration dependence of a transition. We analyzed the Gdm.Cl unfolding transition at three different M_{2-1} concentrations: 0.2, 1, and 10 μM (Figure 4B). Experiments at 10 and 1 μM were monitored by far-UV CD and fluorescence spectroscopy, while experiments at 0.2 μM were followed only by fluorescence spectroscopy because of the low signal-to-noise ratio of CD measurements. The amount of denaturant required for unfolding decreased at lower protein concentrations, confirming that Gdm.Cl-induced M_{2-1} unfolding is coupled to dissociation.

To directly monitor Gdm.Cl-induced M_{2-1} dissociation, we conducted Gdm.Cl unfolding experiments under the same conditions, followed by cross-linking and SDS−PAGE analysis of the resulting species. Unfolding curves at 1 and 10 μM protein were determined, followed by cross-linking with 0.1% glutaraldehyde (see Experimental Procedures), and the samples subjected to SDS−PAGE. During the tetramer to monomer transition (~1.2−2.4 M Gdm.Cl concentration range), we observed mainly only tetrameric and monomeric bands, but no significantly populated dimers or trimers (Figure 5A). At higher Gdm.Cl concentrations, we noticed a small population of a "dimeric" band at 10 μM protein. This band can be explained as a technical artifact resulting from intermolecular cross-linking of the M_{2-1} monomers at higher protein concentrations. Therefore, we consider that the dimeric species is not

dx.doi.org/10.1021/bi200661k | Biochemistry 2011, 50, 8529–8539

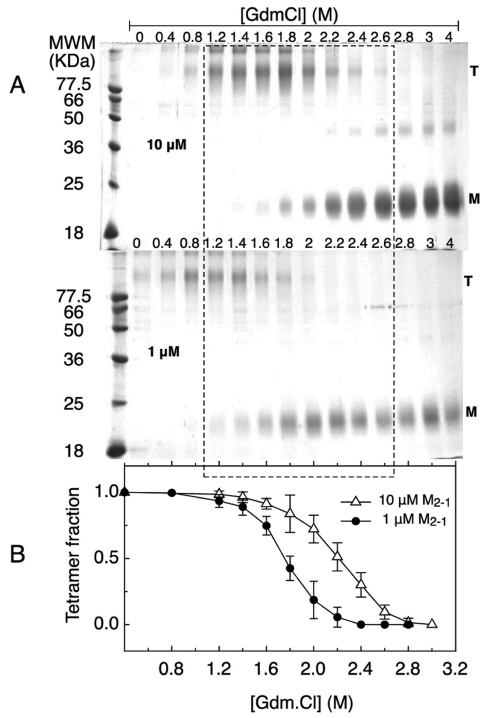

Figure 5. Quaternary structure of M_{2-1} as a function of Gdm.Cl concentration analyzed with glutaraldehyde cross-linking and SDS–PAGE. (A) SDS–PAGE gels showing the quaternary structure of M_{2-1} at two different protein concentrations (1 and 10 μM), as a function of Gdm.Cl concentration (after cross-linking with glutaraldehyde). Lane 1 displays molecular mass markers in kilodaltons. The dashed line indicates the tetramer (T) to monomer (M) transition region, which is shifted to lower Gdm.Cl concentrations as the protein concentration decreases. (B) Densitometric data obtained from the gels, showing the tetramer fraction as a function of Gdm.Cl concentration, at 10 (△) and 1 μM M_{2-1} (●). We consider the small population of the putatively dimeric band observed to be the result of a monomeric intermolecular cross-linking forced by the technique as the protein concentration is increased and not populated in the equilibrium in solution.

populated at equilibrium in solution. On the basis of these results, we neglected the presence of dimeric species in the model proposed below to study M_{2-1} dissociation-unfolding.

The SDS–PAGE bands were scanned densitometrically and used to calculate the tetramer fraction at each Gdm.Cl concentration, which clearly showed the concentration dependence indicative of dissociation (Figure 5B).

M_{2-1} Dissociation-Unfolding takes place via a Monomeric Intermediate. Unfolding of M_{2-1} with urea showed the population of a least one partially folded intermediate (Figure 3). In the case of Gmd.Cl, the CD and fluorescence signals are uncoupled at 1 μM protein, confirming the presence of an intermediate species (Figure 4C). Unlike at 1 μM, the changes in the tertiary and secondary structure of M_{2-1} at 10 μM occurred in parallel within experimental error (Figure 3C). This is not unexpected for a coupled unfolding–dissociation process that is strongly influenced by protein concentration. Next, we combined the results from the cross-linking experiments with the CD and fluorescence unfolding curves at two protein concentrations to reach a quantitative model for M_{2-1} unfolding and dissociation in 50 mM sodium phosphate buffer (pH 7.0) and 1 mM DTT at 20 °C.

We were able to fit the data using an equilibrium model that assumes the population of native tetramers, unfolded monomers, and a monomeric unfolding intermediate:

$$N_4 \overset{K_{D1}}{\longleftrightarrow} 4I \overset{K_{D2}}{\longleftrightarrow} 4D$$

where N_4 is the native tetramer, I is the monomeric intermediate, D is the denatured monomer, and K_{D1} and K_{D2} are the equilibrium constants for each transition (see Experimental Procedures for details). Figure 6 shows the

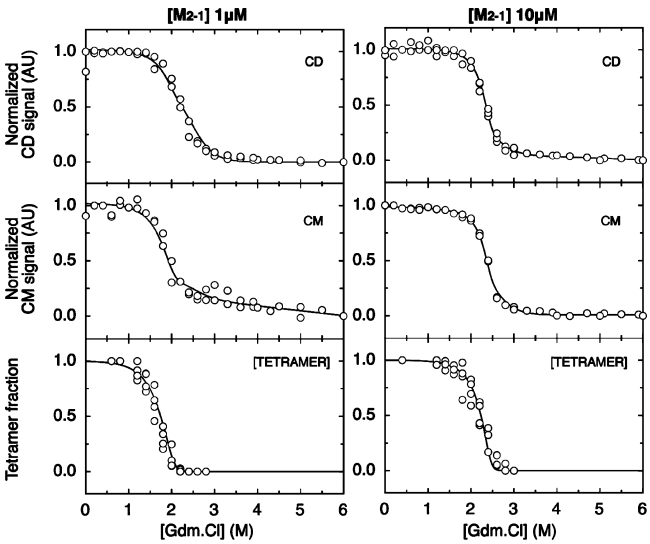

Figure 6. Global fitting of denaturation data to a three-state model considering a monomeric intermediate. The far-UV CD (above), tryptophan center of spectral mass (center), and tetramer fraction (below) signals obtained from equilibrium unfolding experiments performed at 1 (left) and 10 μM (right) M_{2-1} were globally fit to a three-state unfolding model (solid line and see Experimental Procedures). The thermodynamic parameters estimated from the fit are reported in Table 1. CD and fluorescence experiments were repeated two or three times and cross-linking experiments four or five times.

global fittings of the data at 1 and 10 μM, and the thermodynamic parameters estimated from the fit are summarized in Table 1. The process was characterized by a

Table 1. Thermodynamic Parameter Estimates from the Fit Using a Three-State Unfolding Model (see Experimental Procedures)

$N_4 \Leftrightarrow 4I$ equilibrium		$I \Leftrightarrow D$ equilibrium	
$\Delta G_1^{H_2O}$ (kcal/mol)	m_1 (kcal mol^{-1} M^{-1})	$\Delta G_2^{H_2O}$ (kcal/mol)	m_2 (kcal mol^{-1} M^{-1})
−36.8 ± 0.1	6.93 ± 0.03	−5.56 ± 0.02	2.26 ± 0.01

free energy of dissociation from the tetramer to a monomeric intermediate of −36.8 ± 0.1 kcal mol^{-1}, corresponding to a dissociation constant (K_D) of 10^{-28} M^3. The denaturant dependence of the free energy of dissociation, or m value, was 6.93 ± 0.03 kcal mol^{-1} M^{-1}. The monomeric intermediate unfolded into fully denatured monomers with a free energy of −5.56 ± 0.02 kcal mol^{-1} and an m value of 2.26 ± 0.01 kcal mol^{-1} M^{-1}.

Our cross-linking experiments suggested that the intermediate that was populated in the M_{2-1} unfolding transition was

dx.doi.org/10.1021/bi200661k | Biochemistry 2011, 50, 8529–8539

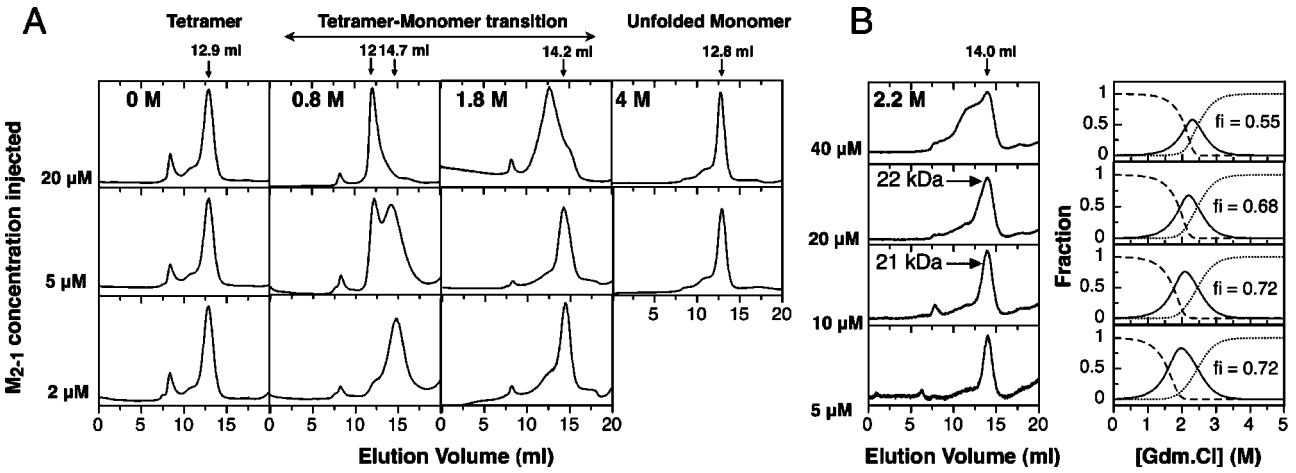

Figure 7. M_{2-1} tetramer unfolding and monomeric intermediate characterization analyzed via size exclusion chromatography and SLS. (A) Size exclusion chromatography of M_{2-1} was conducted on a Superdex 200 column, equilibrated in 50 mM sodium phosphate buffer (pH 7.0) containing the indicated Gdm.Cl concentrations (0, 0.8, 1.8, and 4 M). Samples of M_{2-1} at different protein concentrations (20, 5, and 2 μM) were incubated for 16 h before being run at the appropriate Gdm.Cl concentration. The elution volume of the tetramer, as well as of the unfolded monomer, was ~12.9 mL, and the elution volume of the intermediate was ~14.5 mL. (B) In the left panel, for SLS measurements the sample was incubated at four different protein concentrations (40, 20, 10, and 5 μM) in sodium phosphate buffer (pH 7.0), 1 mM DTT, and 2.2 M Gdm.Cl for 16 h and run on a Superdex 200 column equilibrated at 2.2 M Gdm.Cl. When 20 and 10 μM M_{2-1} was injected, the intermediate species presented a homogeneous peak at 14 mL that could be quantified by SLS, yielding a molecular mass of 22 kDa, corresponding to a monomer. The right panel shows simulations of the fraction of native (---), intermediate (fi, —), and unfolded (···) species according to the three-state unfolding model using the ΔG and m values obtained from the fit shown in Figure 6 (reported in Table 1). Each panel on the right is a simulation at the protein concentration used in the size exclusion experiment shown in the left panel considering a 1/10 sample dilution (i.e., 4, 2, 1, and 0.5 μM from top to bottom, respectively). The fraction of intermediate species (fi) at 2.2 M Gdm.Cl is indicated in each graph.

either a monomer or a tetramer. We investigated this point by conducting SEC experiments at different protein and Gdm.Cl concentrations (Figure 7A). The elution volumes of the native tetramer and the denaturated monomer were 12.9 and 12.8 mL, respectively, at all protein concentrations tested. This similarity is due to the extended conformation of the native tetramer, as shown in Figure 1. At 0 M denaturant, only tetramers were observed, while at 4 M Gdm.Cl, only the unfolded monomer was populated. A third peak with an elution volume of ~14.5 mL appeared in the chromatogram at intermediate Gdm.Cl concentrations (Figure 7A,B). We assign this peak to the partially folded intermediate. SLS of 10 and 20 μM M_{2-1} samples at 2.2 M denaturant yielded a molecular mass of 22 kDa for the intermediate (Figure 7B), confirming that it was a monomer. At all Gdm.Cl concentrations tested (0.8, 1.8, and 2.2 M), the intermediate became less populated at higher total protein concentrations. This is in agreement with the concentration dependence of the unfolding transitions (Figures 3C and 4C) and with simulations of the fractions of native, intermediate, and unfolded species according to our three-state unfolding model (Figure 7B).

Last, we validated our model by using dilution experiments to determine the dissociation constant of M_{2-1}. However, with a K_D of 10^{-28} M^3 in the absence of Gdm.Cl, it was not possible to determine the fraction of the dissociated species by any common spectroscopic lab technique. We conducted the dilution experiments under subdenaturing Gdm.Cl conditions so that dissociation of the M_{2-1} tetramer took place in the low micromolar concentration range. Figure 8A shows that the center of spectral mass can monitor the dissociation as the sample is diluted at three different denaturant concentrations. The data were fit using a two-state dissociation model without populated intermediates:

$$N_4 \overset{K_D}{\leftrightarrow} 4M$$

where N and M are the tetrameric and monomeric species, respectively. Global fitting of the three curves to a tetramer−monomer equilibrium and individual fitting of each curve followed by extrapolation to 0 M Gdm.Cl (Figure 8A, inset) yield a free energies of dissociation of -35.8 ± 0.3 and -34.9 ± 1.4 kcal mol^{-1}, respectively. These values are in excellent agreement with that determined from unfolding experiments, confirming that our dissociation−unfolding model with a monomeric intermediate is an accurate description of the M_{2-1} conformational equilibria in solution.

pH Dependence of M_{2-1} Dissociation. Finally, we investigated whether pH could modulate tetramer formation. For this, we conducted the dilution−dissociation experiments between pH 4.8 and 7.8, at intervals of 0.4 pH unit. Measurements were performed in broad range buffer with 100 mM Tris-HCl, 50 mM MES, 50 mM sodium acetate, and 1 mM DTT at 20 °C. The Gdm.Cl concentration in the buffer solution was varied depending on the pH range, so that dissociation took place in the low micromolar concentration range. Between pH 4.8 and 5.8, measurements were taken in the presence of 0.3 and 0.5 M Gdm.Cl, whereas 1.6 M Gdm.Cl was used between pH 5.8 and 7.8. The measured value for the free energy of dissociation was then extrapolated to 0 M Gdm.Cl using the m value for the dissociation reaction in the three-state model (Table 1).

We observed a strong dependence of the dissociation free energy in this pH range (Figure 8B). With the decrease from pH 7.0 to 5.0, the free energy decreased by more than 13 kcal/mol, corresponding to an increase in K_D from 10^{-28} M^3 at pH 7.0 to 10^{-18} M^3 at pH 5.0. In other words, the tetramer is far weaker at low pH. The data could be fit by a simple model considering coupling of

dx.doi.org/10.1021/bi200661k | Biochemistry 2011, 50, 8529–8539

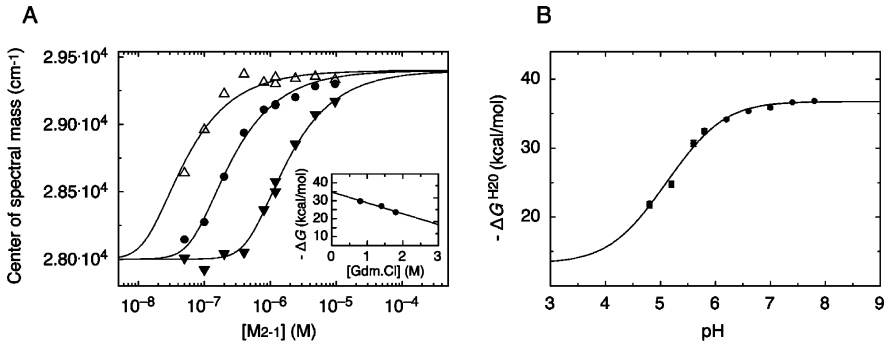

Figure 8. Dilution-induced dissociation of the M_{2-1} tetramer followed by tryptophan fluorescence. (A) Dissociation of the M_{2-1} tetramer at pH 7.0 and at different Gdm.Cl concentrations. The tetramer to monomer transition was followed by the change in the tryptophan center of spectral mass. Serial dilutions of M_{2-1} (from 10 to 0.05 μM) were performed at three different Gdm.Cl concentrations [0.8 (△), 1.4 (●), and 1.8 M (▼)] in 50 mM sodium phosphate (pH 7.0) and 1 mM DTT, incubated for 16 h, and measured at 20 °C. The data were fit to a two-state model considering a single tetramer−monomer equilibrium (solid line and see Experimental Procedures) to obtain the ΔG value at each Gdm.Cl concentration (inset). The ΔG^{H_2O} value obtained from linear extrapolation ($\Delta G^{H_2O} = -34.9 \pm 1.4$ kcal mol^{-1}, and $m = 6.1 \pm 1.0$ kcal mol^{-1}) was in excellent agreement with that obtained by global fitting of the data ($\Delta G^{H_2O} = -35.8 \pm 0.3$ kcal mol^{-1}, and $m = 6.7 \pm 0.4$ kcal mol^{-1}) considering a linear dependence of ΔG on Gdm.Cl concentration. (B) pH dependence of the M_{2-1} tetramer stability. Dilution experiments were performed in broad range buffer at different pH values, and the Gdm.Cl concentration was varied (from 0.3 and 0.5 M for the pH 4.8−5.8 range and 1.6 M Gdm.Cl for the pH 5.6−7.8 range) to allow for measurement of the tetramer−monomer transition. The ΔG values obtained at each pH were extrapolated to 0 M Gdm.Cl using the linear relationship obtained in the experiments at pH 7.0 to obtain the ΔG^{H_2O} value. Stability data were fit (—) considering three titratable residues to obtain the ΔG^{H_2O} value at pH 14.0 ($\Delta G^{H_2O,pH14} = -36.8 \pm 0.1$ kcal mol^{-1}) and the average pK_a values of the residues in the tetrameric (p$K^{Tet} = 4.40 \pm 0.08$) and monomeric (p$K^{Mon} = 5.83 \pm 0.02$) forms (see Experimental Procedures).

the dissociation reaction with the protonation of N residues:[24]

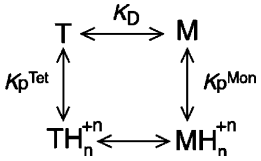

where T and TH_n^{n+} represent the unprotonated and protonated tetramer, respectively, and M and MH_n^{n+} represent the unprotonated and protonated monomer, respectively. Protonation reactions are shown in the vertical direction, where pK^{Tet} and pK^{Mon} are the proton binding constants for the tetrameric and monomeric species, respectively.

Such a model yields the following pH dependence for the dissociation free energy:

$$\Delta G = \Delta G^{pH\,14.0} + N \times 4RT \times \ln\left(\frac{1 + 10^{pK^{Tet}-pH}}{1 + 10^{pK^{Mon}-pH}}\right) \quad (16)$$

where pK^{Tet} and pK^{Mon} are the average pK_a values of the N residues in the tetramer and monomer, respectively.

For the experiments in this work, fitting could be performed considering N values of ≥3. The $N = 3$ fit yielded an average pK^{Tet} of 4.40 ± 0.08 for the group of three titrating residues in the tetramer and an average pK^{Mon} of 5.83 ± 0.02 for the three titrating residues in the monomer. Thus, differential protonation of the M_{2-1} monomer and tetramer strongly favors tetramer dissociation.

DISCUSSION

Viruses in the large Paramyxoviridae family share six fundamental genes and present one to five additional species-specific genes, such as M_{2-1} in pneumoviruses. The M_{2-1} protein plays key functions in RSV as a transcription antiterminator and a mediator of the interaction between the matrix M protein and the nucleocapsid.[12] This prompted us to investigate the biophysical properties of M_{2-1} in solution as a prerequisite for a mechanistic investigation of its interactions with RNA sites and other proteins, and of their consequences in the viral life cycle.

The starting point of this work was the characterization of M_{2-1} conformation in solution at neutral pH. In agreement with previous work,[18] we found that the protein is an α-helical tetramer (Figures 1 and 2). Tran and co-workers reported a globular protein conformation with a diameter of 7.3 ± 0.5 nm.[18] However, the hydrodynamic diameter of M_{2-1} as determined by DLS and SEC experiments was larger than expected for an 88 kDa globular protein and indicative of an extended tetramer (Figure 1). The discrepancy with the published data may come from the different buffers used in the experiments. Tran and co-workers performed their measurements in PBS buffer, whereas in our case, the concentrations of both the salt and the phosphate are higher. This sensitivity of the M_{2-1} conformation to small changes in medium conditions suggests that the protein has the ability to adopt multiple structures. This hypothesis is in agreement with the disruption of the ANS binding site upon addition of nondenaturing concentrations of urea and Gdm.Cl (Figure 3). Because the ANS binding site may well be the same as the RNA binding site, we speculate that the RNA binding properties of M_{2-1} could depend on the conformation populated by the protein.

Next, we studied the conformational behavior of M_{2-1} by perturbing it with denaturants. In the case of Gdm.Cl, we fitted globally spectroscopic (Figure 4) and cross-linking (Figure 5) experiments at two different protein concentrations to obtain a model for the unfolding and dissociation of the M_{2-1} tetramer (Figure 6). According to the model, the native tetramer dissociates into a partly folded monomer that is populated at intermediate Gdm.Cl concentrations. SEC and SLS experiments confirmed this prediction, together with the expected concentration dependence (Figure 7). Moreover, the free

dx.doi.org/10.1021/bi200661k | Biochemistry 2011, 50, 8529–8539

energy of dissociation measured via dilution-induced dissociation experiments is −35.8 ± 0.3 kcal mol^{-1} (Figure 8), in excellent agreement with the value fitted for the model, −36.8 ± 0.1 kcal mol^{-1}. This free energy of dissociation corresponds to a dissociation constant (K_D) of 10^{-28} M^3. This value is close to the K_D of other tight tetramers, such as transthyretin (10^{-34} M^3)[25] or Lac repressor (10^{-30} M^3),[26] and well below the K_D of more labile tetramers, such as p53 (10^{-24} M^3),[21] concanavalin A (10^{-22} M^3),[27] Ssb (10^{-22} M^3),[28] and SecB (10^{-21} M^3).[29]

The monomeric intermediate that is populated during Gdm.Cl-induced M_{2-1} unfolding has interesting properties. First, the SEC experiments indicate that it is more compact than the unfolded monomer (Figure 7). This compact globule unfolds with a change in free energy of 5.6 kcal/mol, which is significant but smaller than the value of 14 kcal/mol expected for a fully folded monomer of 194 residues.[30] The m value for the unfolding reaction is 2.3 kcal mol^{-1} M^{-1}, also smaller than the expected value of 4.9 kcal mol^{-1} M^{-1}.[31] Furthermore, the CD and fluorescence signals of the intermediate lie between those for the native tetramer and the fully unfolded monomer (Figure 6). We find that the monomeric intermediate is consistent with the usual description of a "late molten globule", i.e., a fairly compact globular state with partial secondary and tertiary structure but marginal stability in aqueous solution. As a corollary, formation of the tetramer from the monomeric intermediate involves substantial folding as well as association. We speculate that this coupled folding and binding reaction may play a role in the function of the M_{2-1} protein.

The comparison between urea and Gdm.Cl-induced M_{2-1} unfolding is intriguing. While in urea-induced unfolding the secondary structure is lost before W30 becomes exposed to the solvent (Figure 3), the opposite is true for Gdm.Cl-induced unfolding (Figure 4). In other words, the two denaturants have disparate effects on the secondary and tertiary structure of the protein. This observation further supports the view that M_{2-1} is a malleable polypeptide that may adopt different conformations while fulfilling its multiple functions. The experiments at pH ≤5.0 show that this repertoire of conformations includes higher-order soluble oligomeric species that are large and highly structured (Figure 2).

pH strongly influences the stability of the M_{2-1} tetramer, increasing its dissociation constant, from 10^{-28} M^3 at pH 7.0 to 10^{-18} M^3 at pH 5.0 (Figure 8). We showed that dissociation is coupled with the protonation of at least three residues per monomer (average pK of 5.8) and tetramer (average pK of 4.4). A possible interpretation of this result is that the titrating residues are the same in the monomer and tetramer, and that they are all histidines. Titrating residues would be solvent-exposed in the partially unfolded monomer, leading to the expected pK value near 6. In the tetramer, the deprotonated form would be strongly favored by interactions with other protein groups, thus lowering the pK to a value of 4.4. We speculate that one of the residues may be the zinc binding histidine (His25) in the Cys_3Hys_1 motif.[14] In this case, the histidine would be deprotonated in the tetramer as a requisite for Zn^{2+} coordination. Another one may be His33, which lies in the boundary of the α-helical tetramerization domain.[18] These hypotheses may guide future mutagenesis experiments and the study of related proteins with similar motifs, such as the ebola virus VP30 transcription activator.[13]

As we have shown, lowering the pH strongly destabilizes the M_{2-1} tetramer, inducing dissociation. RSV is an enveloped virus that enters through the cell surface by clathrin-mediated endocytosis, and pH does not affect entry or viability.[32] However, a change in pH could trigger specific changes in M_{2-1} related to its oligomeric state, its interaction with M and N, and its transcription antitermination activity and/or nucleocapsid assembly, all processes in which the protein was shown to participate. Although both the pH values within the cell and the dissociation constant of the tetramer in vivo could be different from those measured in vitro, the extremely strong influence of pH on M_{2-1} conformation suggests that pH-induced conformational changes play a yet to be defined physiological role. It is worth noting that conformational changes induced by modest acidification are likely to play a role in the function of other proteins.[33]

M_{2-1}, unique to pneumoviruses, plays an essential role in virus transcription regulation and in switching off replication through its interaction with the M protein. Investigating its behavior in solution and its ability to interact with other molecules is essential to understanding its mechanisms of action. These equilibria can be described in detailed chemical terms only by perturbing them in vitro. In this work, we set out the basis for investigating zinc binding, dissociation, and oligomerization of M_{2-1} quantitatively. We are hopeful that the study of M_{2-1} conformational equilibria in combination with structural studies, involving protein−protein and protein−RNA interaction, will allow the dissection of biochemical mechanisms underlying the regulation of transcription and genome replication in pneumoviruses.

AUTHOR INFORMATION

Corresponding Author

*E-mail: gpg@leloir.org.ar. Phone: +54 11 5238 7500, ext. 3209. Fax: +54 11 5238 7501.

Present Address

[†]Protein Physiology Laboratory, Departamento de Química Biológica, Facultad de Ciencias Exactas y Naturales, Universidad de Buenos Aires and Consejo Nacional de Investigaciones Científicas y Técnicas de Argentina, C1428EGA Buenos Aires, Argentina.

Funding

This work was supported by Grant CRP/ARG10-02 from the International Centre for Biotechnology (ICGEB). S.A.E., I.E.S., and G.d.P.-G. are Career Investigators from Consejo Nacional de Promocion Cientifica y Tecnologica (CONICET). L.B.C. is the recipient of a postdoctoral fellowship from CONICET.

ACKNOWLEDGMENTS

We thank Nora Lopez for helpful discussions and Gastón Paris for help in SLS measurements and analysis.

ABBREVIATIONS

RSV, respiratory syncytial virus; IPTG, isopropyl 1-thio-β-D-galactopyranoside; SDS, sodium dodecyl sulfate; PAGE, polyacrylamide gel electrophoresis; DTT, dithiothreitol; ANS, 8-anilino-1-naphthalenesulfonate; PAR, 4-(2-pyridylazo)-resorcinol; PMPS, p-hydroxymercuriphenylsulfonate; MES, 2-(N-morpholino)ethanesulfonic acid); Tris, tris(hydroxymethyl)aminomethane; EDTA, ethylenediaminetetraacetic acid; LB, Luria-Bertani; Gdm.Cl, guanidinium chloride; CD, circular dichroism; CM, center of spectral mass.

REFERENCES

(1) Collins, P. L., and Crowe, J. E. (2007) *Respiratory syncytial virus and metapneumovirus*, Lippincott Williams & Wilkins, Philadelphia.

(2) Collins, P. L., Hill, M. G., Camargo, E., Grosfeld, H., Chanock, R. M., and Murphy, B. R. (1995) Production of infectious human respiratory syncytial virus from cloned cDNA confirms an essential role for the transcription elongation factor from the 5′ proximal open reading frame of the M2 mRNA in gene expression and provides a capability for vaccine development. *Proc. Natl. Acad. Sci. U.S.A. 92*, 11563−11567.

(3) Buchholz, U. J., Biacchesi, S., Pham, Q. N., Tran, K. C., Yang, L., Luongo, C. L., Skiadopoulos, M. H., Murphy, B. R., and Collins, P. L. (2005) Deletion of M2 gene open reading frames 1 and 2 of human metapneumovirus: effects on RNA synthesis, attenuation, and immunogenicity. *J. Virol. 79*, 6588−6597.

(4) Grosfeld, H., Hill, M. G., and Collins, P. L. (1995) RNA replication by respiratory syncytial virus (RSV) is directed by the N, P, and L proteins; transcription also occurs under these conditions but requires RSV superinfection for efficient synthesis of full-length mRNA. *J. Virol. 69*, 5677−5686.

(5) Garcia, J., Garcia-Barreno, B., Vivo, A., and Melero, J. A. (1993) Cytoplasmic inclusions of respiratory syncytial virus-infected cells: Formation of inclusion bodies in transfected cells that coexpress the nucleoprotein, the phosphoprotein, and the 22K protein. *Virology 195*, 243−247.

(6) Cartee, T. L., and Wertz, G. W. (2001) Respiratory syncytial virus M2−1 protein requires phosphorylation for efficient function and binds viral RNA during infection. *J. Virol. 75*, 12188−12197.

(7) Mason, S. W., Aberg, E., Lawetz, C., DeLong, R., Whitehead, P., and Liuzzi, M. (2003) Interaction between human respiratory syncytial virus (RSV) M2−1 and P proteins is required for reconstitution of M2−1-dependent RSV minigenome activity. *J. Virol. 77*, 10670−10676.

(8) Collins, P. L., Hill, M. G., Cristina, J., and Grosfeld, H. (1996) Transcription elongation factor of respiratory syncytial virus, a nonsegmented negative-strand RNA virus. *Proc. Natl. Acad. Sci. U.S.A. 93*, 81−85.

(9) Fearns, R., and Collins, P. L. (1999) Role of the M2−1 transcription antitermination protein of respiratory syncytial virus in sequential transcription. *J. Virol. 73*, 5852−5864.

(10) Hardy, R. W., Harmon, S. B., and Wertz, G. W. (1999) Diverse gene junctions of respiratory syncytial virus modulate the efficiency of transcription termination and respond differently to M2-mediated antitermination. *J. Virol. 73*, 170−176.

(11) Hardy, R. W., and Wertz, G. W. (1998) The product of the respiratory syncytial virus M2 gene ORF1 enhances readthrough of intergenic junctions during viral transcription. *J. Virol. 72*, 520−526.

(12) Li, D., Jans, D. A., Bardin, P. G., Meanger, J., Mills, J., and Ghildyal, R. (2008) Association of respiratory syncytial virus M protein with viral nucleocapsids is mediated by the M2−1 protein. *J. Virol. 82*, 8863−8870.

(13) Modrof, J., Becker, S., and Muhlberger, E. (2003) Ebola virus transcription activator VP30 is a zinc-binding protein. *J. Virol. 77*, 3334−3338.

(14) Worthington, M. T., Amann, B. T., Nathans, D., and Berg, J. M. (1996) Metal binding properties and secondary structure of the zinc-binding domain of Nup475. *Proc. Natl. Acad. Sci. U.S.A. 93*, 13754−13759.

(15) Hardy, R. W., and Wertz, G. W. (2000) The Cys_3-His_1 motif of the respiratory syncytial virus M2−1 protein is essential for protein function. *J. Virol. 74*, 5880−5885.

(16) Tang, R. S., Nguyen, N., Cheng, X., and Jin, H. (2001) Requirement of cysteines and length of the human respiratory syncytial virus M2−1 protein for protein function and virus viability. *J. Virol. 75*, 11328−11335.

(17) Cuesta, I., Geng, X., Asenjo, A., and Villanueva, N. (2000) Structural phosphoprotein M2−1 of the human respiratory syncytial virus is an RNA binding protein. *J. Virol. 74*, 9858−9867.

(18) Tran, T. L., Castagne, N., Dubosclard, V., Noinville, S., Koch, E., Moudjou, M., Henry, C., Bernard, J., Yeo, R. P., and Eleouet, J. F. (2009) The respiratory syncytial virus M2−1 protein forms tetramers and interacts with RNA and P in a competitive manner. *J. Virol. 83*, 6363−6374.

(19) Miroux, B., and Walker, J. E. (1996) Over-production of proteins in *Escherichia coli*: Mutant hosts that allow synthesis of some membrane proteins and globular proteins at high levels. *J. Mol. Biol. 260*, 289−298.

(20) Clackson, T., Detlef, G., and Jones, P. W. (1991) *PCR, a Practical Approach*, IRL Press, Oxford, U.K.

(21) Mateu, M. G., and Fersht, A. R. (1998) Nine hydrophobic side chains are key determinants of the thermodynamic stability and oligomerization status of tumour suppressor p53 tetramerization domain. *EMBO J. 17*, 2748−2758.

(22) Uversky, V. N. (2002) Natively unfolded proteins: A point where biology waits for physics. *Protein Sci. 11*, 739−756.

(23) Hunt, J. B., Neece, S. H., and Ginsburg, A. (1985) The use of 4-(2-pyridylazo)resorcinol in studies of zinc release from *Escherichia coli* aspartate transcarbamoylase. *Anal. Biochem. 146*, 150−157.

(24) Baker, B. M., and Murphy, K. P. (1996) Evaluation of linked protonation effects in protein binding reactions using isothermal titration calorimetry. *Biophys. J. 71*, 2049−2055.

(25) Hammarstrom, P., Jiang, X., Deechongkit, S., and Kelly, J. W. (2001) Anion shielding of electrostatic repulsions in transthyretin modulates stability and amyloidosis: Insight into the chaotrope unfolding dichotomy. *Biochemistry 40*, 11453−11459.

(26) Barry, J. K., and Matthews, K. S. (1999) Thermodynamic analysis of unfolding and dissociation in lactose repressor protein. *Biochemistry 38*, 6520−6528.

(27) Sinha, S., Mitra, N., Kumar, G., Bajaj, K., and Surolia, A. (2005) Unfolding studies on soybean agglutinin and concanavalin a tetramers: A comparative account. *Biophys. J. 88*, 1300−1310.

(28) Chilukuri, L. N., Bartlett, D. H., and Fortes, P. A. (2002) Comparison of high pressure-induced dissociation of single-stranded DNA-binding protein (SSB) from high pressure-sensitive and high pressure-adapted marine *Shewanella* species. *Extremophiles 6*, 377−383.

(29) Panse, V. G., Swaminathan, C. P., Aloor, J. J., Surolia, A., and Varadarajan, R. (2000) Unfolding thermodynamics of the tetrameric chaperone, SecB. *Biochemistry 39*, 2362−2369.

(30) Xiao, S., and Raleigh, D. P. (2010) A critical assessment of putative gatekeeper interactions in the villin headpiece helical subdomain. *J. Mol. Biol. 401*, 274−285.

(31) Myers, J. K., Pace, C. N., and Scholtz, J. M. (1995) Denaturant m values and heat capacity changes: Relation to changes in accessible surface areas of protein unfolding. *Protein Sci. 4*, 2138−2148.

(32) Kolokoltsov, A. A., Deniger, D., Fleming, E. H., Roberts, N. J. Jr., Karpilow, J. M., and Davey, R. A. (2007) Small interfering RNA profiling reveals key role of clathrin-mediated endocytosis and early endosome formation for infection by respiratory syncytial virus. *J. Virol. 81*, 7786−7800.

(33) Dawson, J. E., Seckute, J., De, S., Schueler, S. A., Oswald, A. B., and Nicholson, L. K. (2009) Elucidation of a pH-folding switch in the *Pseudomonas syringae* effector protein AvrPto. *Proc. Natl. Acad. Sci. U.S.A. 106*, 8543−8548.